GaAs IMPATT DIODES FOR FREQUENCIES ABOVE 100 GHz: TECHNOLOGY AND PERFORMANCE

H. Eisele, R. K. Mains, G. I. Haddad, C. C. Chen

Center for Space Terahertz Technology
Department of Electrical Engineering & Computer Science
2231 EECS Building
The University of Michigan
Ann Arbor, Michigan 48109-2122

Abstract:

Recent experimental results have demonstrated good performance of GaAs IMPATT diodes around 94 GHz for both output power and noise measure. In this paper the first experimental results and some preliminary theoretical aspects for operation at higher frequencies are given together with an overview of the present status of the device technology. An improved small signal model and especially device simulations clearly depict that the device performance of GaAs IMPATT diodes is strongly limited by the contact resistance at frequencies above 100 GHz. These results agree well with experimental data obtained from W-band (75 - 110 GHz) IMPATT diodes operated at frequencies above their optimum frequency. A maximum output power of 30 mW with an efficiency of 0.73 % was obtained at 105.05 GHz in a W-band cavity. The highest oscillation frequency was 110.2 GHz with 8 mW and 0.2 % efficiency in a D-band cavity. Material parameters of electrons in GaAs for electric fields up to 900 $kVcm^{-1}$ allow a more accurate design of IMPATT diodes for D-band (110 - 170 GHz) operation. Preliminary tests on these IMPATT diodes show pure avalanche breakdown and prove that tunneling is significant only for electric fields above 1.0 $MVcm^{-1}$.

1. Introduction

It has recently been shown that GaAs IMPATT diodes are well suited for W-band operation [1] and exhibit excellent noise performance around 94 GHz [2]. GaAs single-drift flat-profile diodes show a clearly lower noise measure than Si single-drift flat-profile diodes operated in the same type of cavity and tested in the same measurement set up. Compared to Gunn devices these diodes offer better power capabilities, i. e. up to 320 mW, with nearly the same noise measure of 20 dB measured at 10 mW. To date only little is known about the CW performance at frequencies above 100 GHz [3,4].

Therefore, GaAs IMPATT diodes made from a material that was originally designed for 85 to 95 GHz were tested for CW operation at higher frequencies.

2. Design of single-drift flat-profile IMPATT diodes

As pointed out in References 5 and 6 the first derivative of the ionization rates of electrons and holes with respect to the electric field saturates around 500 $KVcm^{-1}$. Together with dead space effects in the avalanche zone [7] this saturation phenomenon favors a flat-profile structure for frequencies above V-band (50 - 75 GHz). The design of the single-drift structure is based on the assumption that the center of the avalanche region occurs where the electron concentration equals the hole concentration [8] for the applied bias voltage and that such a defined avalanche region is electrically equivalent to an avalanche region of the same width l_a but constant electric field and ionization rates [6]. Fig. 1 shows the electric field profile and the carrier concentration calculated for a doping concentration $N_D - N_A = 2.4 \times 10^{17}$ cm^{-3} in the active region at a current density $J_{tot} = 50$ $kAcm^{-2}$ and a junction temperature $T_j = 500$ K. The drift region - where ionization is to be neglected - is defined in its length l_d by the maximum in the well known transit-time function [9]

$$l_d = \frac{3\, v_s}{8 f_o} \quad , \tag{1}$$

where v_s is the average saturated drift velocity (4.5×10^6 cms^{-1} for $T_j = 500$ K) and f_o the operating frequency.

3. Device technology

A selective etching technology for substrateless diodes on diamond heat sinks has successfully been established giving up to 600 diodes per cm^2 wafer area with high uniformity [9]. It implements an AlGaAs etch-stop layer between the substrate and the epitaxial layers for the device. In order to get the steep transitions for doping profiles in the submicron range, all wafers are grown by MBE [1]. Fig. 2 shows the flow chart of this technology process. The epitaxial side of the wafer is metallized with Ti/Pt/Au for a standard p^+-ohmic contact, then selectively plated with gold to form a grating for mechanical support and glued on a ceramic carrier. In the next step the substrate is removed by selective wet chemical etch and subsequently the etch-stop layer in a second selective wet chemical etch. A standard Ni/Ge/Au contact is evaporated on top of the n^+-contact layer and plated with gold. Contact patterns and diode mesas are defined by standard positive photoresist technology and wet chemical etching.

The diodes outside the supporting grating are tested and selected for good d.c. characteristics and exclusively thermocompression bonded on diamond heat sinks for optimum thermal resistance. The diamond heat sinks can be either in the form of copper blocks or similar to the standard ODS 138 packages. Electrical contact to the diode is basically provided by metallized quartz stand-offs thermocompression bonded onto the heat sink and tapered gold ribbons bonded on the diode and the stand-offs. For some diodes metallized quartz rings were very successfully used.

4. Experimental results

RF testing is performed in full height waveguide cavities with a resonant cap on top of the diode both in W-band (WR-10 waveguide) and D-band (WR-6 waveguide).

An output power of 17 mW at 103.8 GHz with an efficiency of 0.54 % and 30 mW at 105.05 GHz with an efficiency of 0.73 % were obtained in a WR-10 waveguide cavity. The highest oscillation frequency of 110.2 GHz could be observed in a WR-6 waveguide cavity. At this frequency the output power was 8 mW and the efficiency 0.2 %.

Table 1 summarizes the experimental results obtained from these diodes. The operating junction temperature was limited up to $T_j = 550$ K in order to ensure reliable long-term operation. As can be seen in Fig. 3 only the efficiency saturates at 6.0 % for 95.4 GHz while the output power monotonically increases up to the maximum bias current. This is also the case for the other results in Table 1 at higher frequencies and it means that the devices are thermally rather than electronically limited.

Table 1: Experimental results in W-band and D-band

Frequency [GHz]	93.4	94.7	95.4	103.8	105.0	110.2
Output power [mW]	140	217	320	17	30	8
Efficiency [%]	4.2	4.5	6.0	0.54	0.73	0.2
Cavity (W/D)	W	W	W	W	W	D

Fig. 4. shows the threshold current density J_{th} as a function of the operating frequency together with the values calculated by means of an IMPATT simulation program based on the drift-diffusion model [11]. Experiment and calculations are in good agreement and will be discussed in the next section.

Using the above discussed design rules, single-drift flat-profile structures for D-band operation were designed and the epitaxial layers grown in an MBE system. Processed devices were tested for d.c. characteristic and doping profile. As depicted in Fig. 5 the breakdown voltages of these IMPATT diodes are in good agreement with the breakdown voltages calculated from ionization rates evaluated in Reference 10. The I-V curve shown in Fig. 6. shows pure avalanche breakdown with a positive temperature coefficient. At present it cannot be determined whether the small leakage current just below breakdown is due to tunneling or surface effects.

5. Device simulation

In order to check the validity of the design at D-band frequencies device structures were simulated in a few preliminary runs using two IMPATT diode simulation programs, a drift-diffusion (DD) model [11] and an energy-momentum (EM) model [12]. Full details of the programs and the material parameters used in these programs will be given elsewhere. In contrast to the experimental results given in [10], slightly higher drift velocities for T_j = 500 K are used and the ionization rates are set equal for electrons and holes. However, the applied ionization rates give nearly the same breakdown voltages as shown in Fig. 5 and additionally, they take the temperature dependence of the breakdown voltages into account that were measured on IMPATT diodes for frequencies from Q-band up to W-band.

As previously mentioned, Fig. 4 shows the calculated J_{th} as a function of the oscillation frequency. As pointed out in [6,13], the oscillation starts at J_{th} when the real part $-R_D$ of the diode impedance $\underline{Z}_D$ just overcomes the series resistance. ($R_L << R_s$, $R_v << R_s$ in the inset of Fig. 4). In this case the series

resistance times unit area $R_s \times A_D$ is assumed to 2×10^{-6} Ωcm^2 as an upper limit and mainly due to the contact resistances in the diode [6]. The improved small signal model in Reference 6 gives similar results. At 140 GHz J_{th} is clearly above the thermal limit of 50 $kAcm^{-2}$ for the W-band diode ($N_D - N_A = 2.4 \times 10^{17}$ cm^{-3} in the active region) and below the expected thermal limit of 60 $kAcm^{-2}$ for one of the D-band diodes ($N_D - N_A = 3.2 \times 10^{17}$ cm^{-3}).

Table 2 shows calculated output power and efficiency at $f = 95$ GHz as preliminary results for both programs. The data for the device area A_D and current density J_{dc} are taken from Reference 1. The energy-momentum program shows slightly higher breakdown voltages and overestimates efficiency and output power. If a series resistance $R_s = 0.18$ Ω is taken into account for this diode, the calculated output power and efficiency agrees very well with the measured values. This series resistance is comparable to the value obtained from small signal impedance measurements in forward direction at 32 MHz [6]. In Table 2 the prediction for one of the D-band structures is included. A smaller $R_s \times A_D$ (1×10^{-6} Ωcm^2) is assumed and demands significantly better technology for contacts on both p^+- and n^+-type GaAs.

Table 2: Calculated results

Area A_D: 8×10^{-6} cm^2 Current density: 50 $kAcm^{-2}$

Model	Voltage [V]	Frequency [GHz]	Power ($R_s = 0$ Ω) [mW]	Efficiency [%]	Power ($R_s = 0.18$ Ω) [mW]	Efficiency [%]
DD	12.2	95.0	550	11.3	320	6.5
EM	12.5	95.0	700	14.0	510	10.2

Area A_D: 5×10^{-6} cm^2 Current density: 60 $kAcm^{-2}$

Model	Voltage [V]	Frequency [GHz]	Power ($R_s = 0$ Ω) [mW]	Efficiency [%]	Power ($R_s = 0.20$ Ω) [mW]	Efficiency [%]
DD	10.4	140.0	120	3.8	35	1.1
EM	10.9	140.0	215	6.5	80	2.4

6. Conclusion

The above discussed experimental results prove that GaAs IMPATT diodes are powerful devices not only for frequencies below 60 GHz, but also above 100 GHz. Together with device simulation high output power can be expected for D-band operation. The simulation also reveals that the contact technology is very crucial for high output power and efficiency and must considerably be improved for GaAs D-band IMPATT diodes.

7. Acknowledgments

This work was supported by the Center of Space Terahertz Technology. A part of the experiments, measurements and calculations were performed by one of the authors (H. E.) at the Lehrstuhl für Allgemeine Elektrotechnik und Angewandte Elektronik, Munich, FRG. The authors are very grateful to Prof. W. Harth for his help.

8. References

[1] Eisele, H., and Grothe, H.: "GaAs W-band IMPATT diodes made by MBE", *Proc. MIOP '89*, Sindelfingen, FRG, Feb. 28th - March 3rd 1989, Session 3A.6.

[2] Eisele, H.: "GaAs W-band IMPATT diodes for very low-noise oscillators", *Electronics Letters*, **26**, 1990, pp. 109-110.

[3] Elta, M. E., Fettermann, H. R., Macropoulos, W. V., and Lambert, J.: "150 GHz GaAs MITATT source", *IEEE Trans. Electron. Device Lett.*, **EDL-1**, 1980, pp. 115-116.

[4] Chang, K., Kung, J. K., Asher, P. G., Hayashibara, G. M., and Ying, R. S.: "GaAs Read-type IMPATT diode for 130 GHz CW operation", *Electronics Letters*, **17**, 1981, pp. 471-473.

[5] Rolland P. A., Friscourt M. R., Lippens D., Dalle C., and Nieruchalski, J. L.: "Millimeter Wave Solid-State Power Sources", *Proc. of the International Workshop on Millimeter Waves*, Rome, April 2-4, 1986, pp. 125-177

[6] Eisele, H.: "GaAs W-Band IMPATT diodes: The first step to higher frequencies", *Microwave Journal*, to be published.

[7] Okuto, Y., and Crowell, C. R., "Threshold energy effects on avalanche breakdown voltage in semiconductor junctions", *Solid-State Electron.*, **18**, 1975, pp. 161-168

[8] Hulin, R.: "Großsignalmodell von Lawinenlaufzeitdioden", Ph.D. Thesis Techn. University Braunschweig, Braunschweig 1973

[9] Eisele, H.: "Selective etching technology for 94 GHz GaAs IMPATT diodes on diamond heat sinks", *Solid-State Electronics*, **32**, 1989, pp. 253-257.

[10] Eisele, H.: "Electron properties in GaAs for the design of mm-wave IMPATTs", *Int. Journal of Infrared and Millimeter Waves*, **4**, 1991, to be published.

[11] Bauhahn, P. E., and Haddad, G. I.: "IMPATT device simulation and properties", *IEEE Trans. Electron Devices*, **ED-24**, 1977, pp. 634-642.

[12] Mains, R. K., Haddad, G. I., and Blakey, P. A.: "Simulation of GaAs IMPATT Diodes Including Energy and Velocity Transport Equations", *IEEE Trans. Electron. Devices*, **ED-30**, 1983, pp. 1327-1338

[13] Adlerstein, M. G., Holway L. H., and Chu, S. L. G.: "Measurement of Series Resistance in IMPATT Diodes", *IEEE Trans. Electron Devices*, **ED-30**, 1983, pp. 179-182

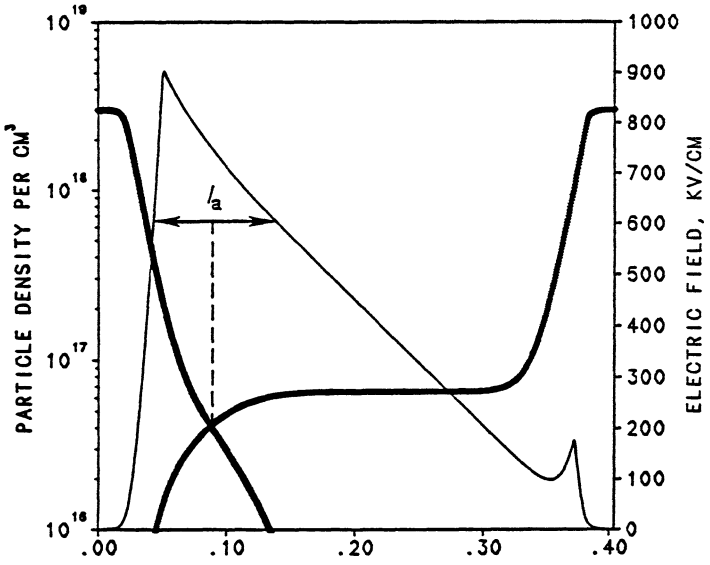

Fig. 1: Electric field E, electron and hole concentration n, p as a function of space x for $N_D - N_A = 2.4 \times 10^{17}$ cm^{-3} in the active region.

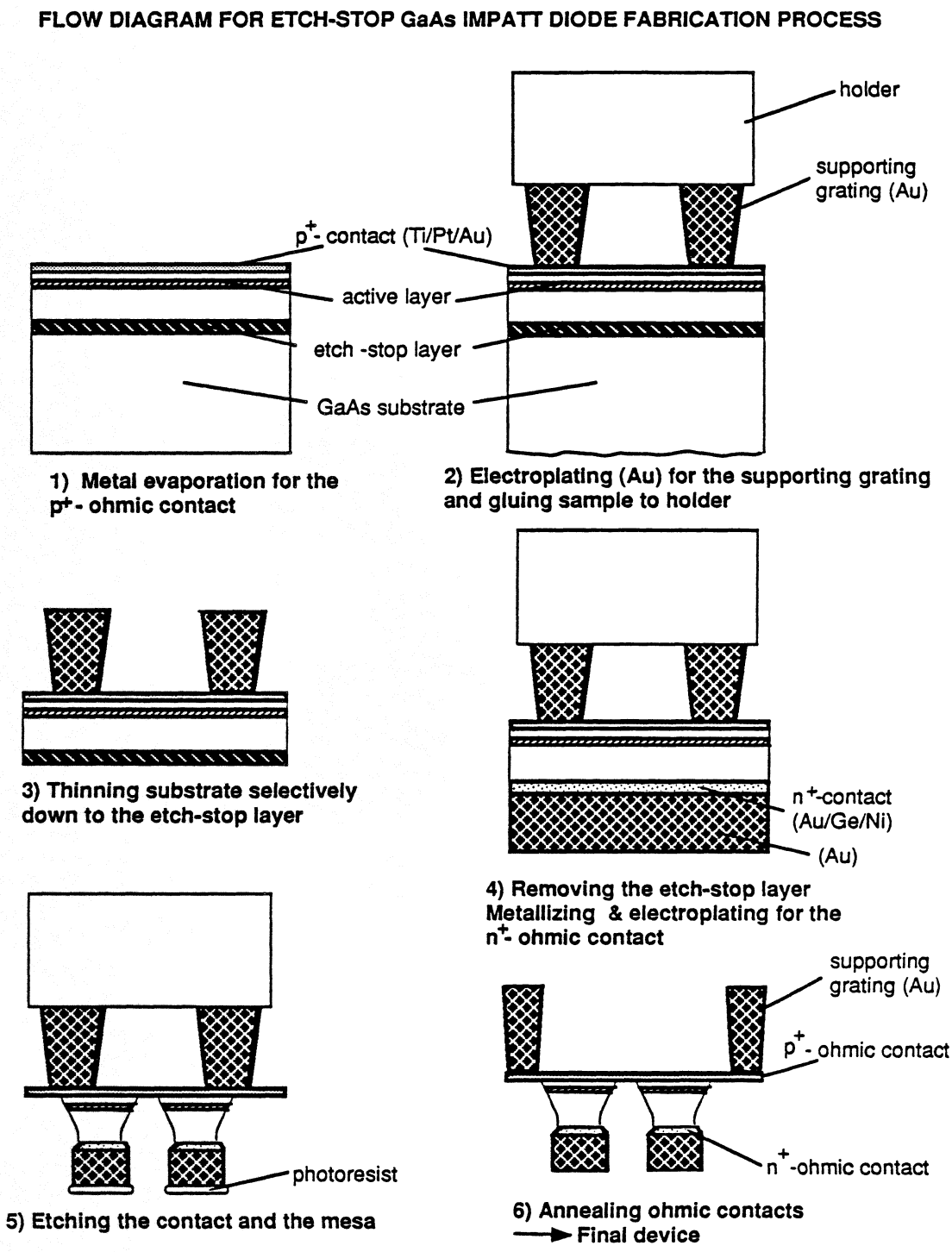

Fig. 2: Flow chart for IMPATT diodes device fabrication.

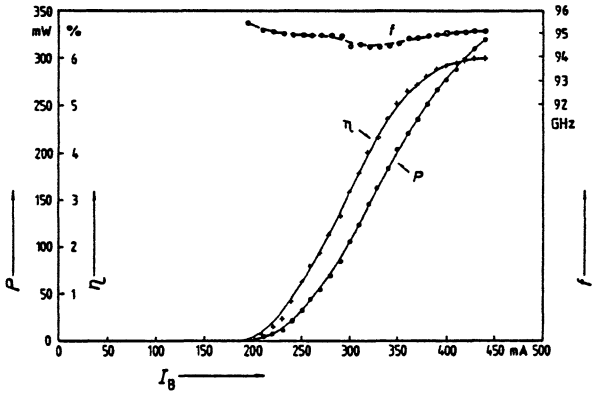

Fig. 3: Performance of a GaAs W-band single-drift flat-profile IMPATT diode.

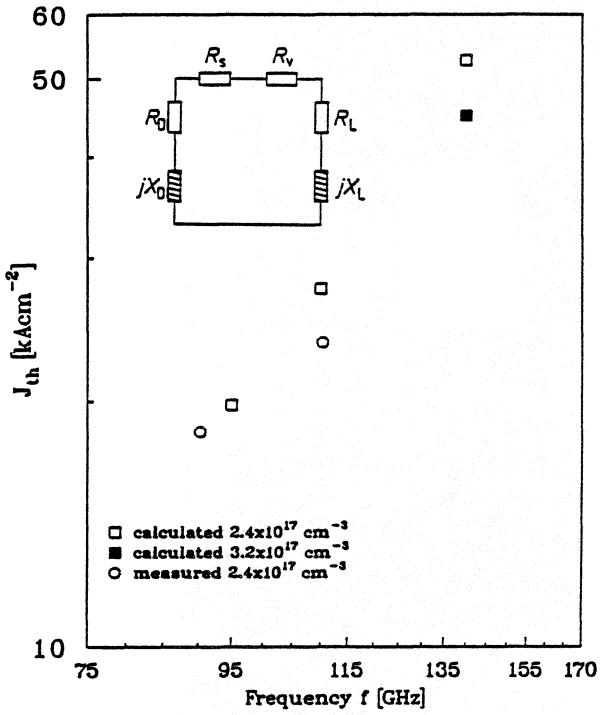

Fig. 4: Measured and calculated threshold current density J_{th} as a function of frequency for W-band and D-band single-drift flat-profile IMPATT diodes.

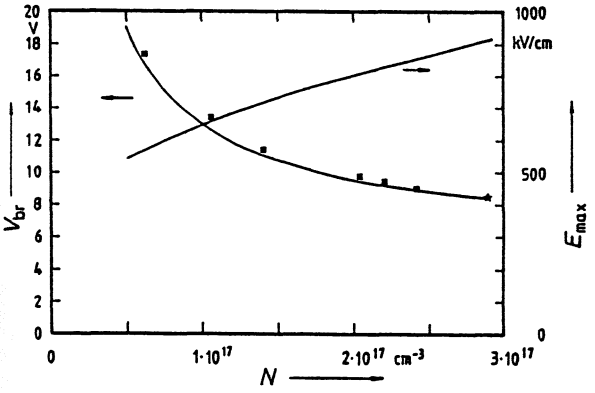

Fig. 5: Breakdown voltage V_{br} and peak electric field E_{max} of an abrupt p$^+$n-junction.
■ ★ : measured
—— : calculated.

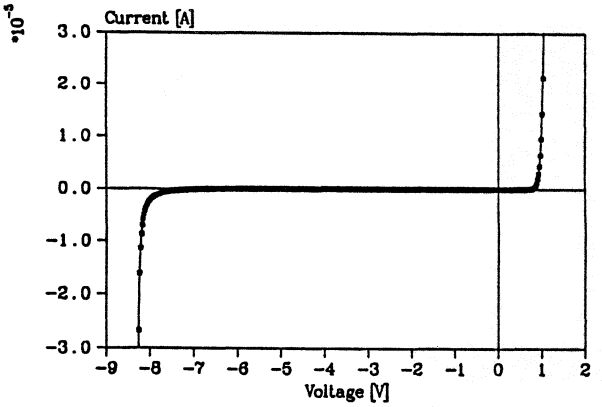

Fig. 6: I-V-curve of a D-band IMPATT diode with N_D - N_A = 2.9 × 10^{17} cm^{-3} in the active region.